Supplementary Materials for

Theory-Guided Development of a Barium-Doped Cobalt Catalyst for Ammonia Decomposition

A. Gunnarson[#], A. Cao[#], O. F. Sloth[#], M. Varón, R. Bueno Villoro, T. Veile, C. D. Damsgaard, C. Frandsen, J. K. Nørskov[*], I. Chorkendorff[*]

*Corresponding authors. Email: icho@dtu.dk, jkno@dtu.dk

[#]These authors have contributed equally.

1. Theoretical section

Density functional theory (DFT) calculation method

DFT calculations were performed using the Vienna *Ab initio* Simulation Package (VASP),[1,2] employing the generalized gradient approximation (GGA)[3] with the Revised PBE (RPBE) functional.[4] Valence electrons were described by the plane-waves with an energy cutoff of 450 eV, whereas core electrons were represented by projector augmented-wave pseudopotentials (PAW).[5]

For bulk and all surface calculations, Monkhorst-Pack k-point grid[6] of 12 × 12 × 12 and 2 × 2 × 1 was used. A lattice constant optimization was performed on the HCP bulk structure of Co. The ($10\bar{1}5$) surface was generated using 4-layer 4 × 6 cells to represent the stepped surface on Co based on our previous models.[7] The resulting unit cell had six by four surface atoms and included two steps per unit cell. 15 Å of vacuum separated the slabs in the z-direction, and dipole correction was applied. The bottom two layers of each slab were constrained to their original positions, while the upper layers were allowed to relax. All slabs and bulk were relaxed until all forces converged to less than 0.05 eV. The electronic energy convergence criterion was 10^{-5} eV.

Transition states (TS) of the reactions were located by the climbing image nudged elastic band (Cl-NEB) method[8] with at least five images generated between the initial and final states. The TS structures obtained by this method were further refined until the forces on atomic centers reached 0.05 eV $Å^{-1}$. Zero-point energies and entropic contributions were calculated within the harmonic approximation. Free energy corrections of gas-phase species were obtained using the Shomate equation.[9]

The formation energy of adsorbed species (M*/(MO)*/(MOH)*/(MN)*/(MH)*) on the metal surface was calculated by

$$\Delta E(\text{species}) = E(\text{slab+M+H}_x\text{O}_y\text{N}_z) - E(\text{slab}) - \text{E(M)} - xE_{\text{H}} - yE_{\text{O}} - zE_{\text{N.}} \quad (1)$$

where E(slab+M+$H_xO_yN_z$) and E(slab) mean the electronic energy of species (M+$H_xO_yN_z$) adsorbed on the metal Co surface and the electronic energy of the pristine Co surface, respectively. E(M) is the electronic energy of a single promoter M atom, which refers to the Nb bulk energy. $E_H = 0.5E_{H2}$, $E_O = E_{H2O} - E_{H2}$, and $E_N = E_{NH3} - 1.5E_{H2}$ are relative to the respective gas-phase energies, and x, y, and z are chosen to represent the number of hydrogen, oxygen, and nitrogen atoms in the adsorbed intermediate. H_2 gas phase values were corrected by adding 0.09eV as described in ref[10].

The adsorption energy of N_xH_y * is calculated by

$$\Delta E(N_xH_y) = E(\text{slab}+N_xH_y) - E(\text{slab}) - xE_N - yE_H \quad (2)$$

where $E(\text{slab}+N_xH_y)$ and $E(\text{slab})$ mean the electronic energy of species (N_xH_y) adsorbed on the surface and the electronic energy of the surface, respectively. $E_H = 0.5E_{H2}$ and $E_N = E_{N2}$ are relative to the respective gas-phase energies, and x, and y are chosen to represent the number of nitrogen and hydrogen atoms in the adsorbed intermediates. H_2 gas phase values were corrected by adding 0.09eV as described in ref[10].

The free energy (ΔG) is given by

$$\Delta G = \Delta H - T\Delta S = \Delta E + \Delta E_{zpe} + \int_0^T CpdT - T\Delta S \quad (3)$$

where ΔE means ΔE (species), ΔE (bulk), or ΔE (TS). E_{ZPE} is the zero-point energy correction, ΔH is the enthalpy correction, ΔS is the entropy change, Cp is heat capacity, and T is the absolute temperature.

The activity volcano for ammonia synthesis as a function of the transition state energy and N adsorption energy is established using CATMAP software[11] and micro-kinetic modelling[12].

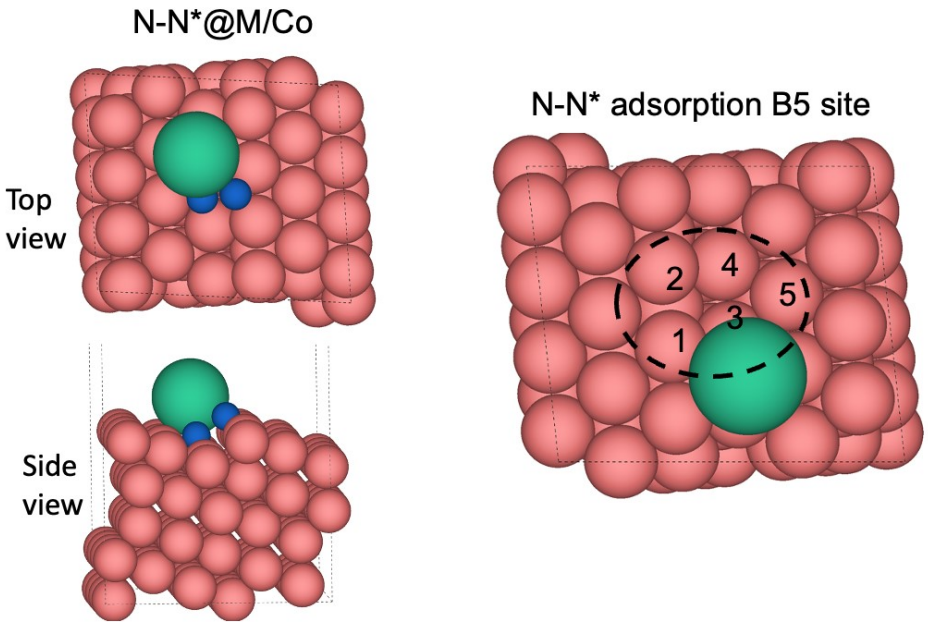

Fig S1.1 The calculation on promoter-induced spin moment change. The configurations of the transition state for N-N coupling (left) and the example of Co atoms at the B5 active site. The spin moment change on these five Co atoms = total spin moment on these five Co atoms (with promoter) - spin moment on these five Co atoms (without promoter).

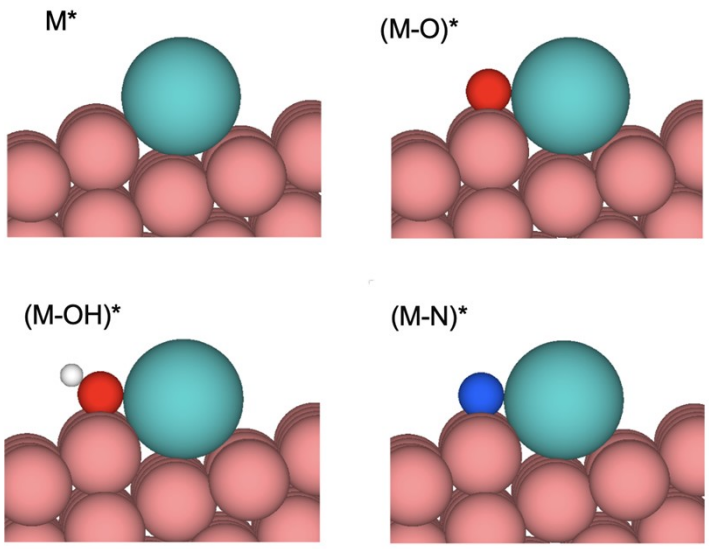

Fig S1.2 Structural models for adsorbed M*/(MO)*/(MOH)*/(MN)*/(MH)* on the stepped Co($10\bar{1}5$) surface. Green, pink, red, white and blue spheres represent promoter, Co, O, H, and N atoms, respectively.

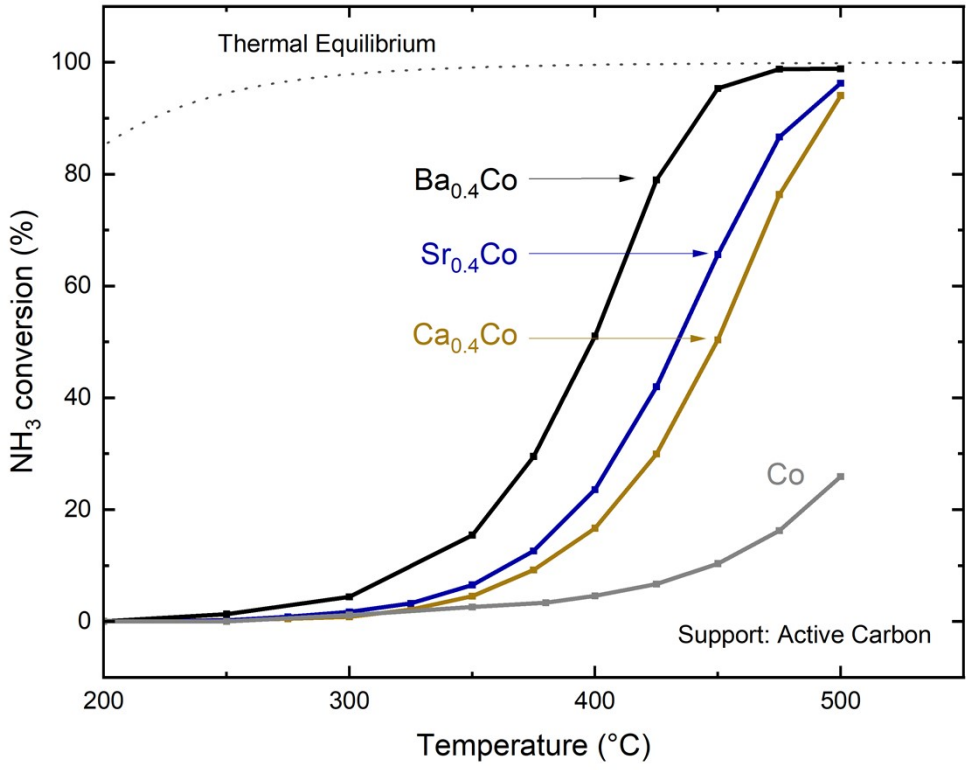

Fig S1.3 Experimental comparison of cobalt catalysts (10 wt.% Co on active carbon) promoted by Ba, Sr, and Ca. The atomic ratio of M/Co was 0.4 (M = Ba, Sr, Ca). As discussed in the main text, a higher performance of Sr- and Ca-based catalysts is expected but could not be achieved due to the high stability of the promoter oxides, which cannot be reduced under our reaction conditions (see the phase diagrams in **Fig. 1b-d**).

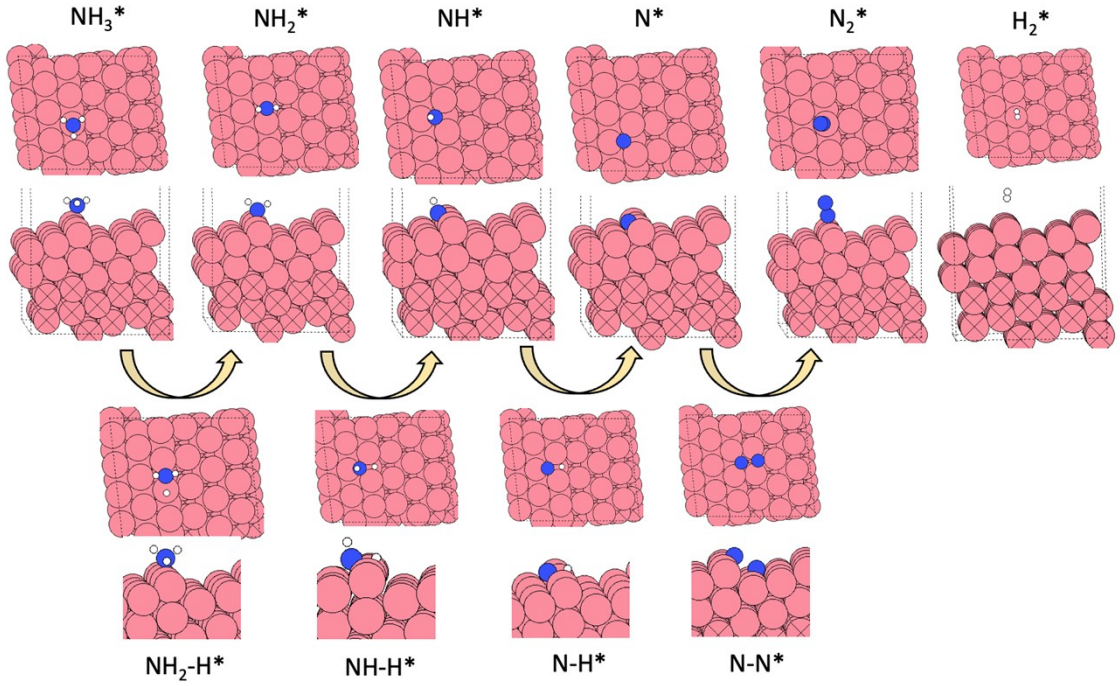

Fig S1.4 Reaction mechanism on Co. Reaction paths of ammonia decomposition on Co, where pink, blue, and white spheres represent Co, N, and H, respectively.

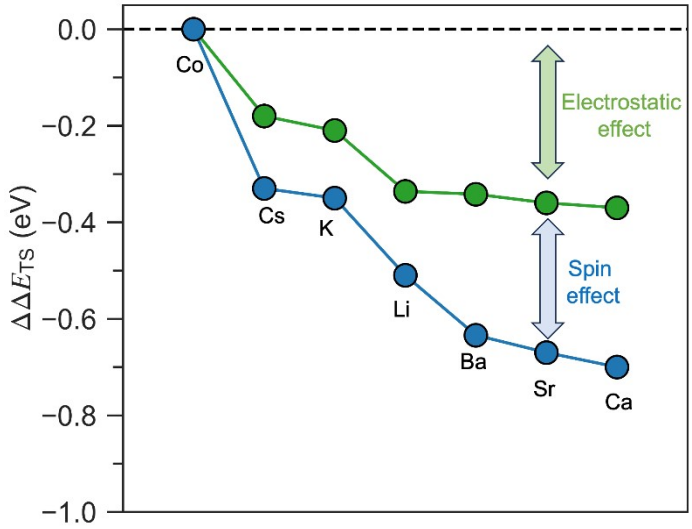

Fig S1.5 The change in transition state (TS) energy of N-N-coupling induced by the electrostatic and the spin effect of various promoters in comparison to an unpromoted Co surface (ΔΔETS = ΔE_{TS}(with promoter) – ΔE_{TS}(without promoter)).

2. Experimental section

Catalyst preparation

The synthesis was based on the work of Hagen et. al.[13]: The carbon support (Norit ROW, Alfa Aesar) was activated by heating it to 1100 °C in reducing atmosphere of 10 vol.% H_2 in N_2 for 48 h. The salts $Co(NO_3)_2 \cdot 6H_2O$ (Sigma-Aldrich), $Ba(CO_2CH_3)_2$ (Alfa Aesar), $Ni(NO_3)_2 \cdot 6H_2O$ (Thermo Scientific Chemicals) and $RuCl_3 \cdot xH_2O$ (Sigma-Aldrich) were subsequently impregnated dropwise onto to dry carbon support. Ba was impregnated individually after deposition of the base metal. The catalysts were dried in air at RT for 1 h, 60 °C for 6 h and 120 °C for 18 h after the addition of base metal and Ba. The catalyst precursors were investigated by ICP-MS to determine the metal loading:

Table S1 Summary of the metal content of the catalyst precursors.

Sample ID	Precursor Metal content by ICP-MS (wt.%)				Metal (Co,Ni,Ru) used in the reaction (mg)	Ba used in the reaction (mg)	Ba/M ratio
	Co	Ni	Ru	Ba			
Co/C	7.8 ± 0.1	0	0	0	12.5	0.0	0
$Ba_{0.01}Co/C$	8.5 ± 0.1	0	0	0.2 ± 0.0	13.6	0.3	0.01
$Ba_{0.02}Co/C$	9.3 ± 0.1	0	0	0.4 ± 0.0	14.9	0.6	0.02
$Ba_{0.1}Co/C$	7.4 ± 0.0	0	0	1.8 ± 0.0	11.8	2.9	0.10
$Ba_{0.2}Co/C$	8.6 ± 0.1	0	0	3.9 ± 0.1	13.8	6.2	0.19
$Ba_{0.4}Co/C$ - B1	7.4 ± 0.1	0	0	6.0 ± 0.1	11.8	9.6	0.35
$Ba_{0.4}Co/C$ - B2	7.7 ± 0.0	0	0	6.5 ± 0.1	12.3	10.4	0.36
$Ba_{0.6}Co/C$	6.7 ± 0.1	0	0	9.6 ± 0.1	10.7	15.4	0.61
Ba/C	0	0	0	8.2 ± 0.1	0.0	13.1	-
Ni/C	0	8.1 ± 0.1	0	0	13.0	0.0	0.00
$Ba_{0.02}Ni/C$	0	8.3 ± 0.0	0	0.4 ± 0.0	13.3	0.6	0.02
Ru/C	0	0	5.0 ± 0.1	0	8.0	0.0	0.00
$Ba_{0.1}Ru/C$	0	0	4.5 ± 0.1	0.5 ± 0.0	7.2	0.8	0.08
C (reference)	0	0	0	0	0.0	0.0	-

Catalyst testing

Setup

The testing setup is shown in **Fig S2.1**.

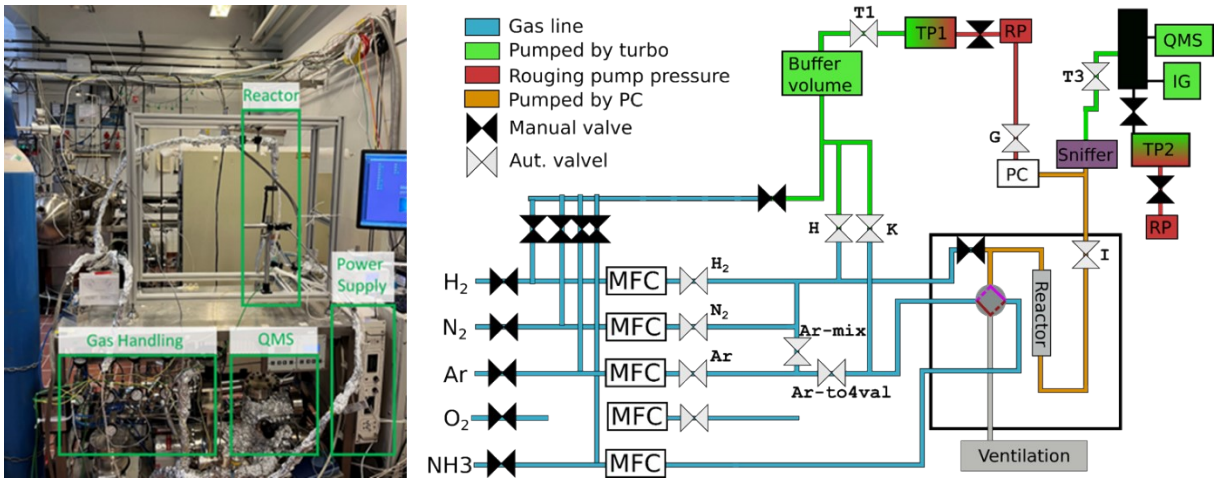

Fig. S2.1 Overview of the testing setup. A photo of the setup is shown on the left, while a schematic drawing is provided on the right.

If not stated otherwise, 160 mg of catalyst precursor were deposited into 4.9 mm inner diameter FeCrAl reactors. The bed length was 1.0 ± 0.1 cm, supported by approximately 0.5 cm of quartz wool on either side. If not stated otherwise, a flow of pure (6.0) ammonia of 10 mL min^{-1} (GHSV = 3750 mL g_{cat}^{-1} h^{-1}) was used. The catalytic activity was evaluated by scanning the ammonia conversion in dependence of temperature in two evaluation cycles. Firstly, the catalyst was cycled from RT to 500 °C in steps of 25 °C. All steps were held for 20 min. Since especially the promoted catalysts activated significantly during this procedure, a second cycling from RT to 625 °C, again in steps of 25 °C was performed afterwards and used for the evaluation of the catalysts. The setup is heated resistively by a current passed through two copper clamps fixed onto the reactor. Subsequently, the reactor is encased in a quartz wool insulation of approx. 5 cm on all sides.

Calibration

The ammonia conversion was assessed by mass spectrometry. Part of the reaction mixture was taken from the gas stream through a so-called sniffer to a QMS chamber. To calculate the NH_3 concentration in the stream from the MS signal S_{MS}, a calibration was performed (**Fig S2.2**). Fitting the points of NH_3 with a polynomial, the ammonia conversion C_{NH3} was calculated as follows:

$$S_{MS,N} = S_{MS}/S_{MS,PureNH_3}$$

$$C_{NH_3}(\%) = \left(1 - 0.109 * S_{MS,N}^{4} + 0.767 * S_{MS,N}^{3} - 1.790 * S_{MS,N}^{2} + 2.132 * S_{MS,N}\right) * 100$$

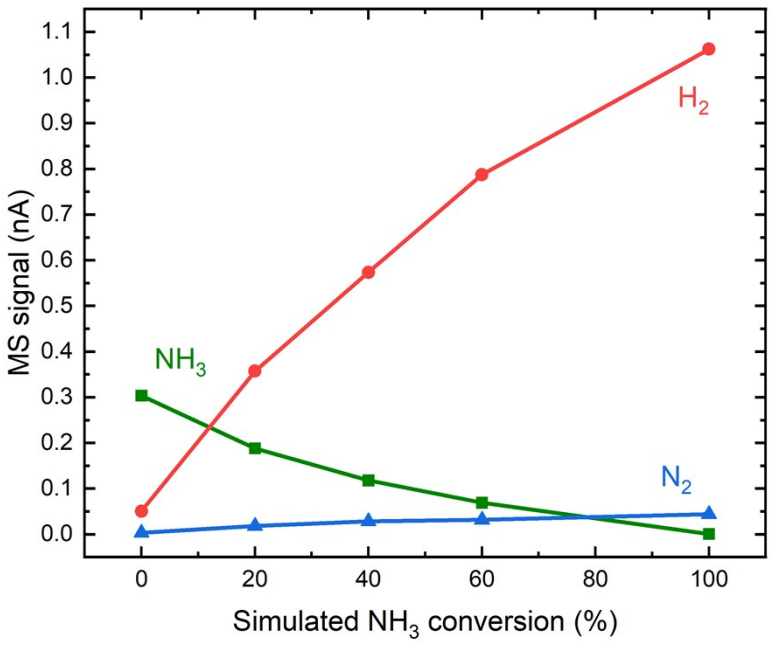

Fig. S2.2 Calibration performed to calculate the NH_3 conversion from the MS signal (M/Z = 17). To simulate the conversion, pure (6.0) NH_3 was diluted with a 3:1 mixture of H_2:N_2.

Temperature monitoring

In this work, we generally measure the temperature using a thermocouple (Pro K-type, RS) within the catalyst bed. The thermocouple is coated with a dense MgO layer, preventing contact with the gas atmosphere. Blank experiments were conducted with several different thermocouples, confirming the inertness. To compare the temperature in- and outside the reactor and to validate the measured temperature, we further welded several thermocouples to the outside of the reactor (**Fig S2.3**). The temperature is comparable, although the outside surface seems to be about 10 – 20 °C hotter than the inside of the reactor. Possible reasons may be the cold ammonia flow and the endothermic reaction at higher temperatures.

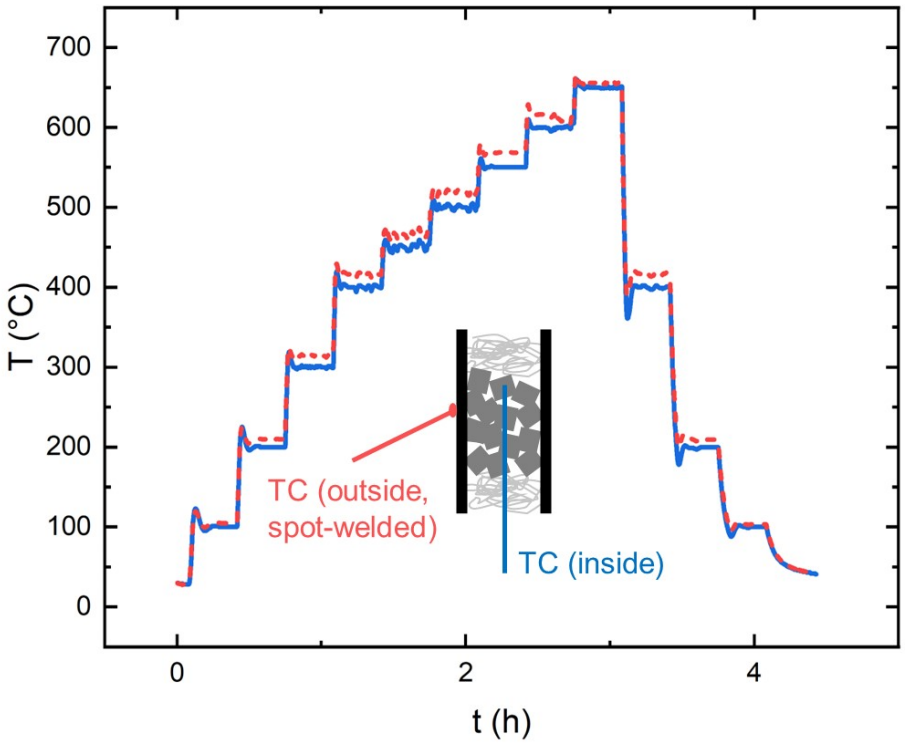

Fig S2.3 Comparison of thermocouples (TC) in- and outside the reactor. The red dotted line presents the average of three thermocouples welded to the $_{outside}$ surface of the reactor using spot welding.

Blank measurement

Recently, Gómez-Cápiro et al. investigated the blank activity of different reactor materials for ammonia decomposition.[14] They found an activation of most steels through cycling in ammonia to a temperature of 600 °C. Therefore, we conducted blank test experiments consisting of longer holding periods at relevant temperatures, including cycling and exposing of the reactor to air (at RT). The temperature ramp and related ammonia conversion activity of a reactor filled with carbon support is shown in **Fig S2.4**.

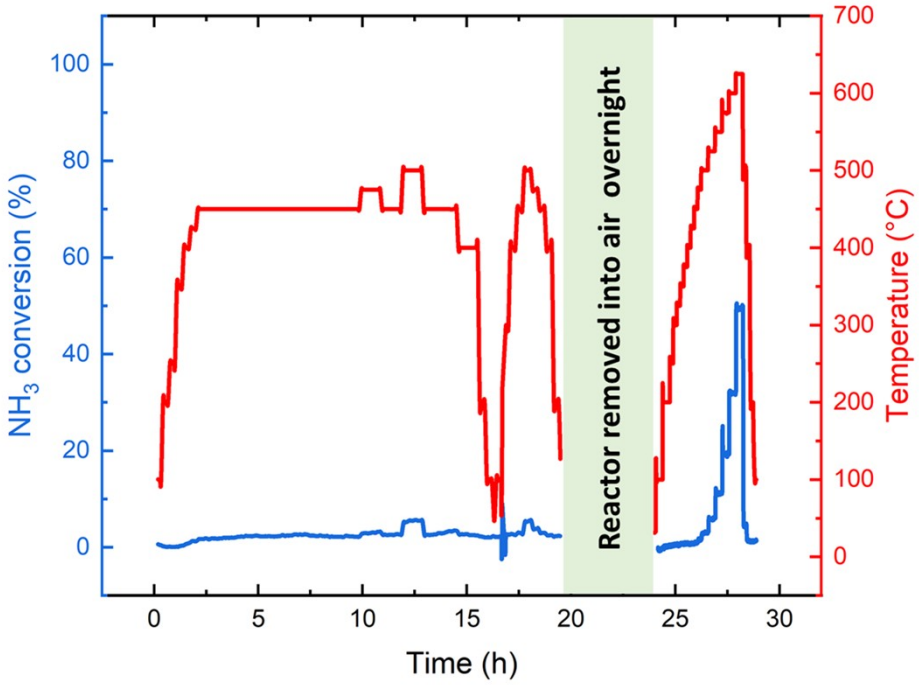

Fig S2.4 Blank experiment conducted with a kanthal reactor filled with 160 mg of carbon support.

The blank measurement indicates that even after a long activation period and cycling, a low conversion of ~5 % is observed at 500 °C. Considering that the catalysts developed in this study reach full conversion at 450 – 475 °C, we do not expect a significant contribution of the reactor to the overall activity.

Raw data and methane formation

As described previously, the ammonia conversion is quantified by mass spectrometry. The last 5 minutes of the 20 min intervals at the individual temperatures are averaged and converted to a conversion (see *calibration*) using a python script. An example of the raw data, also indicating the methane formation (M/Z = 15) above 500 °C, is shown in **Fig S2.5**.

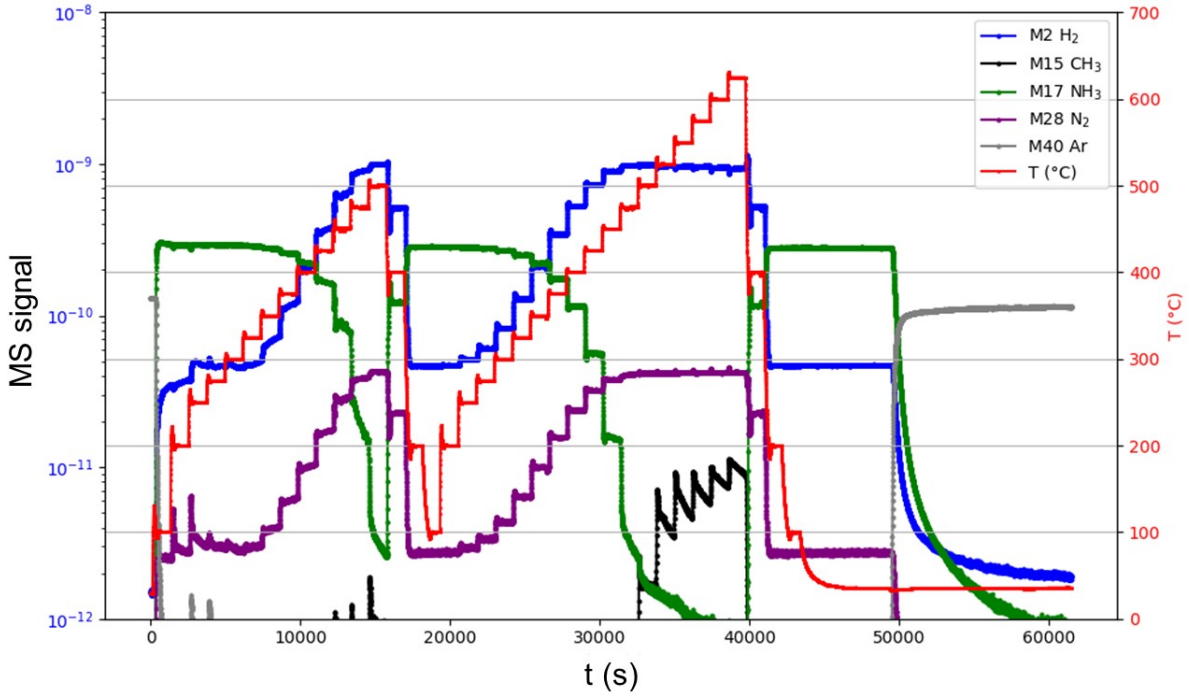

Fig S2.5 Example of the raw data recorded during the evaluation of $Ba_{0.4}Co$ consisting of time, temperature and MS signal, which is evaluated using a python script.

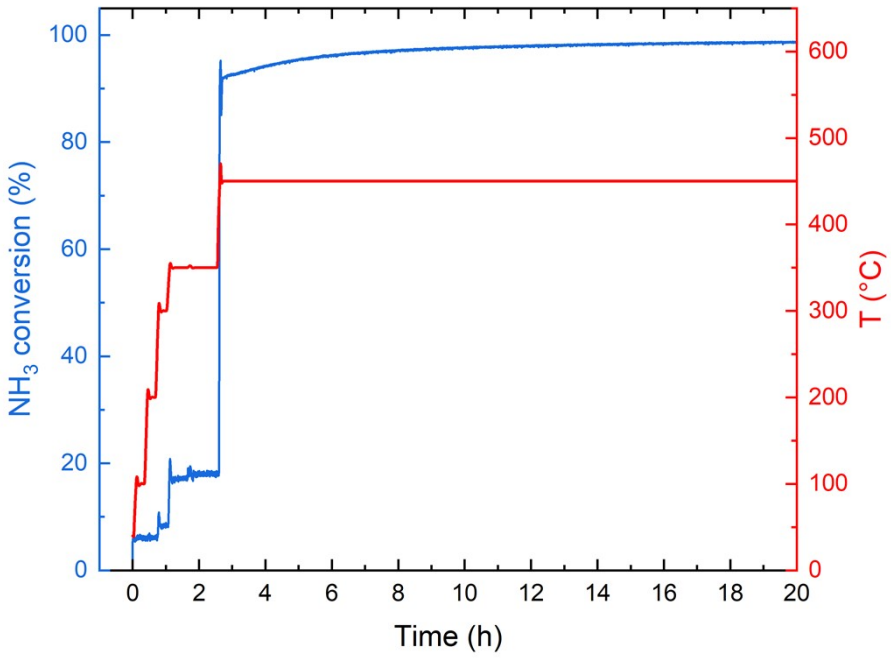

Fig S2.6 Alternative activation of the $Ba_{0.4}Co$ catalyst by holding a temperature of 450 °C in an NH_3 flow of 10 mL min^{-1}.

Calculation of the TOF

The TOF was calculated based on the surface/volume-averaged (Sauter) diameter, which is calculated from the total volume and the total surface area of a particle population as follows:

$$d_{Sauter} = 6 \cdot \frac{V_{total}}{A_{total}}$$

The total surface area of Co $A_{Co,total}$ can then be calculated from the total Co mass $m_{Co,total}$ and the mass $m_{Co,NP}$ and surface area $A_{Co,\,NP}$ of one Co nanoparticle having the Sauer diameter:

$$A_{Co,total} = \frac{A_{Co,\,NP} \cdot m_{Co,total}}{m_{Co,NP}}$$

To calculate the number of active sites, the cobalt area was multiplied by the Co surface density of 15.2 Co atoms per nm^2. The latter was determined by averaging the surface densities of the facets (111), (110) and (100) and is in a common range for surface densities found experimentally.[15,16] Alternatively, the TOF can be calculated only considering cobalt atoms contained in so-called B5 sites as active sites. It was recently shown that such sites contribute to most of the catalytic activity.[17] The amount Co atoms forming B5 sites on a nanoparticle of a given size and FCC crystal structure can be calculated based on Wulff-constructions by:

$$\frac{\#_{Co,B5}}{\#_{Co,total}} = 1.16 \cdot d_{Sauter}{}^{-1.80}$$

The TOF is then calculated based on the number of active sites $\#_{Act}$, the conversion C_{NH_3} and ammonia flow F_{NH_3} as follows:

$$TOF = \#_{Act} \cdot C_{NH_3} \cdot F_{NH_3}$$

An ideal Ba loading can be calculated considering that only one atom of Ba is required per B5 site:

$$\left(\frac{\#_{Ba}}{\#_{Co,total}}\right)_{ideal} = \frac{\#_{Co,B5}}{\#_{Co,total} \cdot 5}$$

Analysis by HAADF-STEM and STEM-EDX

The scanning transmission electron microscopy was carried out on a Thermo fischer scientific spectra ultra microscope operated at 300 kV, a convergence angle of 24 mrad, a HAADF collection angle of 73-200 mrad and a camera length of 109 mm. To reduce noise, 10 frames were summed with a dwell time of 2 µs per frame. The magnification calibration was verified using the interplanar spacings of a standard gold calibration sample.

EDX maps were acquired using an ultra-X detector for approx. 30 minutes per map. Multivariate statistical analysis was performed for noise reduction and the Cliff–Lorimer formula was used for elemental quantification.[18]

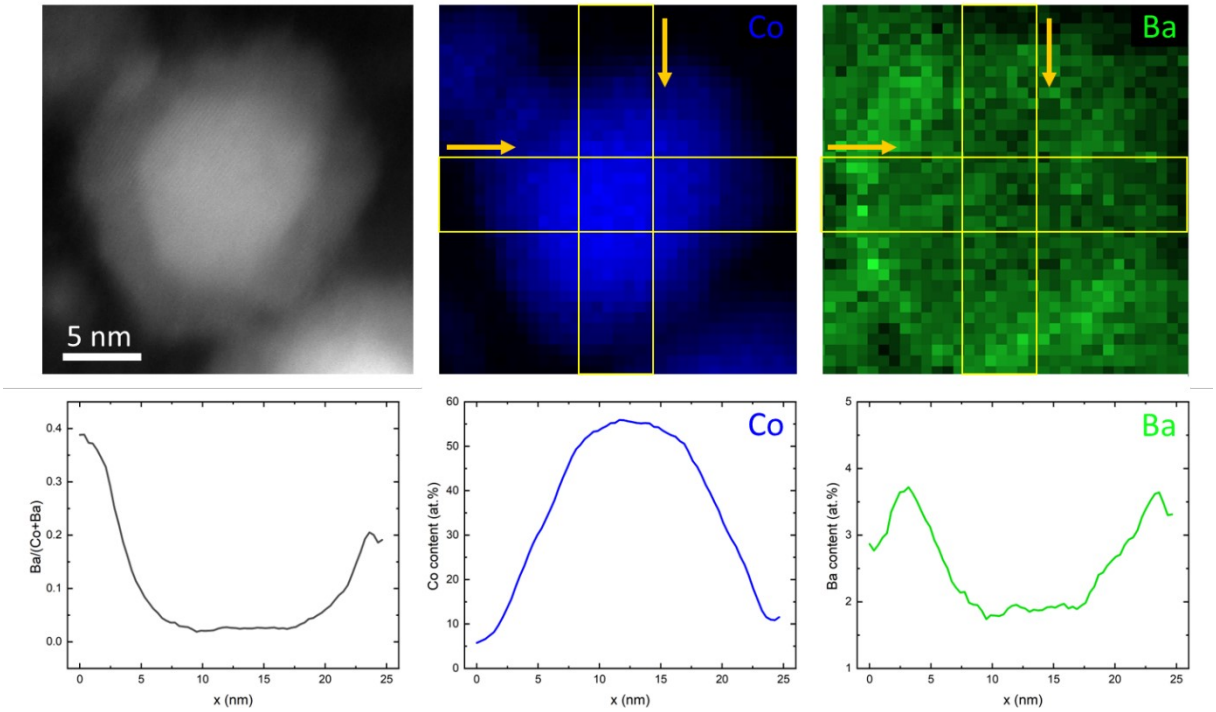

Fig S2.7 Detailed analysis of an exemplary STEM-EDX micrograph of the spent $Ba_{0.4}Co$ catalyst. The Co and Ba distribution is shown in the form of a concentration profile following the yellow areas indicated in the above images. The horizontal and vertical concentration profiles were averaged.

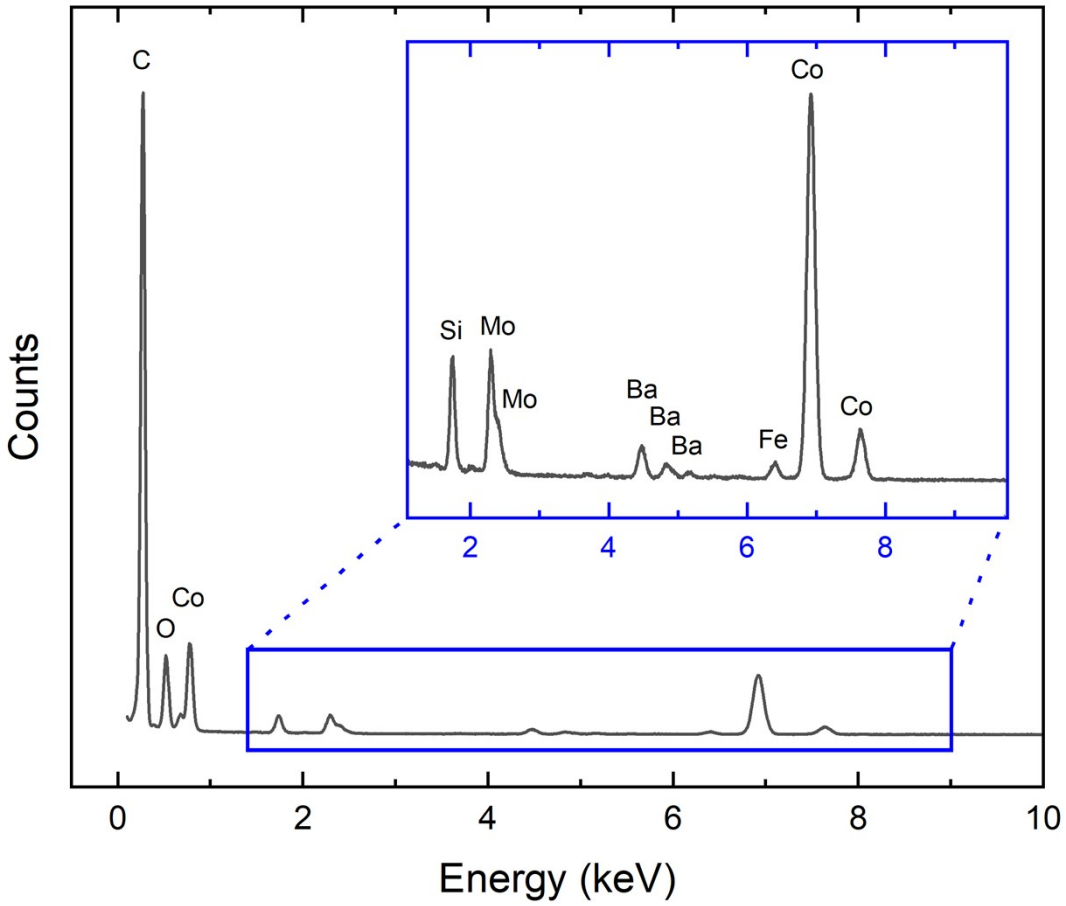

Fig S2.8 EDX spectrum recorded for the micrograph indicated in Fig S2.7. The sample was investigated on a molybdenum grid coated with lacey carbon. The silicon signal is attributed to the presence of quartz wool, which cannot be separated completely from the spent catalyst.

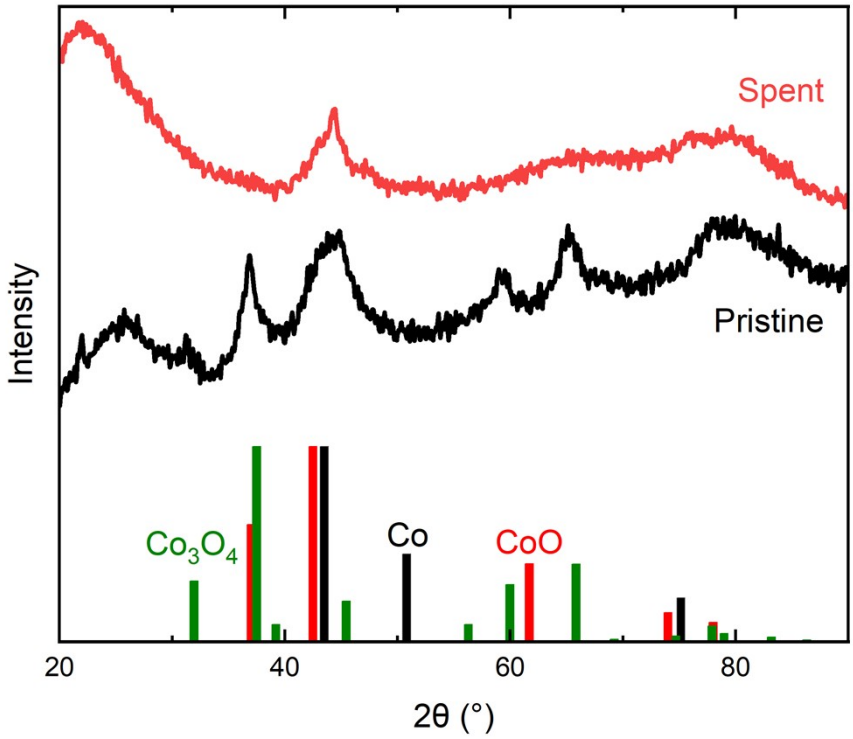

Fig S2.9 XRD pattern of the $Ba_{0.4}Co$ catalyst investigated by STEM-EDX before (red) and after (black) the testing for > 60 h under reaction conditions. The reference patterns were taken from the ICSD database.

1 G. Kresse and J. Furthmüller, *Comput. Mater. Sci.*, 1996, **6**, 15–50.

2 G. Kresse and J. Hafner, *Phys. Rev. B*, 1993, **47**, 558–561.

3 J. P. Perdew, K. Burke and M. Ernzerhof, *Phys. Rev. Lett.*, 1996, **77**, 3865–3868.

4 J. Wellendorff, K. T. Lundgaard, A. Møgelhøj, V. Petzold, D. D. Landis, J. K. Nørskov, T. Bligaard and K. W. Jacobsen, *Phys. Rev. B Condens. Matter Mater. Phys.*, 2012, **85**, 32–34.

5 P. E. Blöchl, *Phys. Rev. B*, 1994, **50**, 17953–17979.

6 H. Monkhorst and J. Pack, *Phys. Rev. B*, 1976, **13**, 5188–5192.

7 B. A. Rohr, A. R. Singh and J. K. Nørskov, *J. Catal.*, 2019, **372**, 33–38.

8 G. Henkelman, B. P. Uberuaga and H. Jónsson, *J. Chem. Phys.*, 2000, **113**, 9901–9904.

9 C. H. Shomate, *J. Phys. Chem.*, 1954, **58**, 368–372.

10 A. A. Peterson, F. Abild-Pedersen, F. Studt, J. Rossmeisl and J. K. Nørskov, *Energy Environ. Sci.*, 2010, **3**, 1311–1315.

11 A. J. Medford, C. Shi, M. J. Hoffmann, A. C. Lausche, S. R. Fitzgibbon, T. Bligaard and J. K. Nørskov, *Catal. Letters*, 2015, **145**, 794–807.

12 A. R. Singh, J. H. Montoya, B. A. Rohr, C. Tsai, A. Vojvodic and J. K. Nørskov, *ACS Catal.*, 2018, **8**, 4017–4024.

13 S. Hagen, R. Barfod, R. Fehrmann, C. J. H. Jacobsen, H. T. Teunissen, K. Ståhl and I. Chorkendorff, *Chem. Comm.*, 2002, **11**, 1206–1207.

14 O. Gómez-Cápiro, S. Ristig, J. Folke and H. Ruland, *Energy Technol.*, 2024, **12**, 2300996.

15 A. Y. Khodakov, R. Bechara and A. Griboval-Constant, *Appl. Catal. A Gen.*, 2003, **254**, 273–288.

16 F. Borji, A. N. Pour, J. Karimi, M. Izadyar, Z. Keyvanloo and M. Hashemian, *Prog. React. Kinet. Mec.*, 2017, **42**, 89–98.

17 K. Zhang, A. Cao, L. H. Wandall, J. Vernieres, J. Kibsgaard, J. K. Nørskov and I. Chorkendorff, *Science*, 2024, **383**, 1357–1363.

18 S. Zhang and C. Scheu, *Microscopy*, 2018, **67**, i133–i141.